

promoting access to White Rose research papers



Universities of Leeds, Sheffield and York
<http://eprints.whiterose.ac.uk/>

This is the author's post-print version of an article published in **Review of Scientific Instruments**

White Rose Research Online URL for this paper:

<http://eprints.whiterose.ac.uk/id/eprint/78199>

Published article:

Wood, CD, Mistry, D, Li, LH, Cunningham, JE, Linfield, EH and Davies, AG (2013) *On-chip terahertz spectroscopic techniques for measuring mesoscopic quantum systems*. Review of Scientific Instruments, 84 (8). 085101. ISSN 0034-6748

<http://dx.doi.org/10.1063/1.4816736>

On chip terahertz spectroscopic techniques for measuring mesoscopic quantum systems

C. D. Wood, D. Mistry, L. H. Li, J. E. Cunningham, E. H. Linfield and A. G. Davies

School of Electronic and Electrical Engineering, University of Leeds, Leeds LS2 9JT, UK.

Abstract:

We present the self-aligned fabrication of on-chip devices in which waveguides, incorporating integrated photoconductive switches, are combined with two-dimensional electron systems to allow probing of the ultrafast (terahertz frequency range) properties of confined semiconductor systems, both at cryogenic temperatures and in high magnetic fields. We demonstrate the direct injection of on-chip terahertz pulses into the mesoscopic system by femtosecond, near infra-red laser excitation of in-plane photoconductive switches formed on an epitaxially grown, low-temperature-grown GaAs layer, which is integrated monolithically with a GaAs / AlGaAs heterostructure containing a two-dimensional electron system. Both the input and output terahertz signals of an on-chip waveguide are sampled by altering dynamically the photoconductive excitation / detection arrangement *in situ* on a single device. We also demonstrate a new method for sub-Kelvin excitation and detection of on-chip terahertz frequency radiation in a $^3\text{He} / ^4\text{He}$ dilution refrigerator that allows the photocurrent and detected terahertz transient to be mapped as function of the near-infrared excitation position at the emitter and detector, respectively. Furthermore, we demonstrate transmission of terahertz transients through a two-dimensional electron system in a coplanar waveguide under magnetic field at temperatures as low as 200 mK.

I. INTRODUCTION:

As the drive toward faster electronics forces a reduction in device dimensions, understanding the ultrafast, quantum behaviour of charge carriers in the mesoscopic regime becomes increasingly important. The physics of mesoscopic systems, such as the two-dimensional and one-dimensional electron systems (2DES / 1DES) formed in GaAs / AlGaAs heterostructures, is governed by the inter-subband spacing and Coulomb charging energies, with characteristic values of typically 1 – 10 meV. Experiments, therefore, require the use of sub-Kelvin temperatures, to suppress thermal fluctuations and allow full understanding of the underlying quantum mechanical properties. Furthermore, under application of a strong magnetic field, dynamic *in situ* quantisation of the density of states is possible, resulting in terahertz (THz) frequency carrier dynamics such as cyclotron resonance,¹ bulk magnetoplasmon oscillations,² and edge magnetoplasmons.³ Correspondingly, the timescales of many transient events, such as carrier transport through asymmetric double-barrier systems⁴ and ballistic transport through nanoscale mesoscopic systems⁵ are of order 1 – 100 ps. Experiments in the THz frequency range (0.1 – 10 THz; 0.4 meV – 40 meV) are therefore increasingly of fundamental interest for the study of such ultrafast carrier dynamics. However, many of these phenomena have yet to be explored fully at THz frequencies at the required milli-Kelvin temperatures and high magnetic fields, owing to the difficulties in developing suitable experimental measurement methodologies.

The generation of ultrafast THz transients typically relies on near-infrared (NIR), femtosecond pulsed excitation of a biased photoconductive (PC) switch, which is often formed on low-temperature-grown GaAs (LT-GaAs). The resultant THz radiation is emitted into free-space where it is used to probe the THz properties of materials placed in its propagation path, before it is sensed coherently using, for example, electro-optic techniques. In this way, THz-frequency measurements of cryogenically cooled quantum-confined semiconductor systems, including

2DESs,⁶ quantum cascade laser (QCL) heterostructures⁷ and quantum dots^{8, 9} have been probed using free-space THz time-domain spectroscopy (THz-TDS). Such studies, however, highlight the need to maximize the interaction between the sample and the probing THz radiation, which is limited by the thickness (for example, when measuring 2DESs) and cross-section (for example, when measuring quantum dots) of the mesoscopic systems. Indeed, in the latter case, the use of dense assemblies, to improve signal-to-noise ratios, necessarily leads to an ensemble-averaged measurement.

In contrast, the use of on-chip THz devices offers the possibility of integrating a *single* mesoscopic or nanoscale device into a wave guiding structure (and therefore to the device being directly accessed by a propagating THz pulse). This increases significantly interactions between the THz field and the device, and removes ensemble contributions to the THz response. In this case, in-plane PC switches, biased using surface electrodes, are coupled to an overlaid, planar waveguiding structure. Instead of radiating into free space, the resultant THz transients couple into and propagate along the planar waveguide, and will interact with devices or materials placed within or close to the waveguiding structure.

Previously, a number of on-chip THz devices have been demonstrated at cryogenic temperatures, including those based on superconducting waveguides,¹⁰ microstrip lines¹¹ and coplanar waveguides (CPWs)¹², with the latter geometry better suited to device integration owing to the planar configuration of both the signal conductor and ground planes. These experiments, however, relied upon excitation of the integrated PC switches using NIR lasers focussed through optical access windows of a cryostat. Black-body thermal loading therefore typically limits these measurements to a maximum temperature of ≈ 1.2 K in ^4He cryostats, and to ≈ 0.4 K in ^3He systems.¹³

Local delivery of NIR laser pulses to the on-chip THz waveguide is, however, also possible using optical fibres,¹⁴ introduced into the cryostat via apertures much smaller than optical windows and positioned away from the sample chamber. Owing to the low thermal coupling along the fibres ($\approx 8 \mu\text{Wm}^{-1}$ from 300 K to 4.2 K) compared to the typical cooling power of a dilution refrigerators (mW at a few hundred mK), the aforementioned temperature limitation is mitigated.

Other practical limitations do, though, impede sub-Kelvin THz measurements of single mesoscopic systems. For example, aligning an individual mesoscopic / nanoscale device with an on-chip sensing region presents a significant fabrication challenge. Furthermore, cryogenic measurements of fibre-coupled on-chip THz waveguides^{3, 14, 15} have traditionally been complicated by difficulties in positioning the optical fibres optimally relative to the planar photoconductive switches, necessary in order to maximise the generated DC photocurrent and hence the THz signal generation. Specifically, to illuminate the PC switches effectively, each fibre must be aligned carefully above the appropriate switch at a fixed height (typically 10s of microns depending on the fibre numerical aperture and switch size). In previous studies, the fibres were secured in position using UV-curable transparent adhesive. Unfortunately, misalignment of the PC switches can then arise: firstly, during the adhesive curing stage, and second, from differential thermal contraction between the fibres, adhesive and sample surface during thermal cycling of the cryostat. Furthermore, in the ideal scenario, it is important to have the ability to measure both the input signal (i.e. the THz signal generated prior to propagation down the transmission line) and output signal (after propagation down the transmission line) of each device, allowing normalisation of a pulse transmitted through, for example, an integrated mesoscopic system between different measurements and samples. This requirement highlights an implicit limitation of gluing fibres onto the sample – excitation of closely spaced (10s of μm separation) PC switches is not possible, owing to the size of the optical fibre (typically $> 100 \mu\text{m}$, including cladding). This has hitherto restricted experiments to a single excitation / detection arrangement for each device.

In this paper, we present an experimental arrangement which allows in-situ translation and optimization of the NIR pump and probe pulse positions relative to the surface of a THz guided-wave device with sub-micron accuracy, and which allows the pump and probe beams to be aligned with the same PC switch. The apparatus can operate inside a dilution refrigerator, providing access to both input and output THz signals of a single device at sub-Kelvin temperatures. The technique allows dynamic compensation for sample misalignment during cooling or upon application of an external magnetic field, and also allows the first full position-dependant map of excited THz transients to be generated. In parallel, we have developed a new MBE-grown layer arrangement for monolithically integrating a photoconductive material (LT-GaAs) with a 2DES heterostructure, which allows the fabrication of individual, self-aligned 2DES-containing mesas with an overlaid on-chip THz device.

II. METHODOLOGY

A. Optical arrangement

The generation and detection of on-chip THz transients was based on the well-established technique of terahertz time-domain spectroscopy.¹⁶ A 70 fs pulsewidth, 80 MHz pulsed Ti:Sapphire laser centered at 780 nm was used to excite and detect THz radiation in our experiments. The laser pulses were first negatively pre-chirped using a pair of ruled gratings with a blaze angle of 19° 23' arranged in a near-Littrow configuration to compensate for fibre dispersion. The NIR pulses were then separated into pump and probe beams using an ultrafast beam splitter, and optically chopped for lock-in detection, before being focussed into two 10 m lengths of solid core silica fibre using aspheric lenses. The resultant pulse widths at the ends of the fibres were 130 fs (limited by non-linear effects in the fibre), as measured by an autocorrelator.

The fibres were passed into the top of a closed-cycle $^3\text{He} / ^4\text{He}$ dilution refrigerator through ferrules which were sealed using GE varnish. Inside the refrigerator, the fibres were thermally

clamped at each temperature stage to minimise heat conduction, before being terminated below the mixing plate in brass ferrules pivoted at the mixing plate surface (Figure 1). The emitted laser light was collimated using aspheric lenses attached to the ends of the ferrules, the lower end of each ferrule being clamped to two orthogonal linear piezoelectric stages. These allowed each collimated laser pulse to be scanned dynamically with submicron-scale precision over an area of $\sim 5 \text{ mm}^2$, across the surface of the on-chip waveguide mounted $\sim 30 \text{ cm}$ below, at the center of a 12 T superconducting magnet. A plano-convex lens fixed above the sample, focused the pump and probe beams onto the sample surface where they could be aligned with the excitation and detection PC switches.

For THz measurements, the pump and probe NIR beams were attenuated to 1 mW average power, to ensure that the cooling power of the dilution refrigerator (4 mW at 200 mK) was not exceeded. Although the small THz pulse amplitude arising from the low NIR excitation powers can, in principle, be compensated by increasing the PC switch bias, we observed significant THz pulse broadening at switch biases above $\sim 15 \text{ V}$, which adversely affected bandwidth. We attribute this to a combination of sample heating, and a reduction in the electron capture cross section of Coulombic attractive donor states, which correspondingly increases the LT-GaAs electron lifetime.¹⁷ All PC switches were therefore biased at a fixed value of 10 V DC, resulting in $\approx 1 \mu\text{A}$ generated photocurrent.

B. Devices and materials

To facilitate integration of a mesoscopic system with a THz waveguide, we chose to use a coplanar waveguide (CPW) geometry (Figure 2). The CPWs consisted of Ti / Au (10 / 200 nm) metallization, thermally evaporated through a lithographically-defined mask onto the surface of an LT-GaAs layer.

CPWs are known to support two fundamental modes of propagation: the desired coplanar mode

and a more lossy, dispersive slotline mode. To discriminate between these modes in the transmitted THz pulse, two pairs of PC switches (each measuring $5\ \mu\text{m} \times 30\ \mu\text{m}$) were defined on opposite sides of the center conductor, at either end of a 1.2-mm-long CPW region. Extension of the CPW on either side of the PC switch regions served to remove THz pulse reflections during time-domain measurements. An on-chip THz signal was generated by illuminating switch 1 or 2 using a pulsed NIR laser, and biasing the appropriate switch using the adjacent parasitic probe arm. The transmitted signal was probed using a second, time-delayed NIR laser pulse illuminating switch 3 or 4, and measured using lock-in detection. The change in sign of the slotline mode when measured at switch 3 with respect to switch 4 (owing to asymmetry of the electric field about the center conductor) allowed discrimination between the two propagating modes using a technique similar to that used by Zamdmer *et al.*¹⁸, although here we are able to sample each component individually rather than as a convolution. The maximum theoretical device bandwidth was estimated to be ~ 1 THz, as calculated from the ground-signal-ground separation ($20\ \mu\text{m} - 30\ \mu\text{m} - 20\ \mu\text{m}$) and the dielectric constant of GaAs (≈ 12.3).

The use of LT-GaAs as the PC switch material offers the prospect of integrating monolithically a GaAs / AlGaAs 2DES with the LT-GaAs layer during epitaxial growth. Previous studies have demonstrated incorporation of a 2DES beneath an LT-GaAs layer for freespace THz measurements of cyclotron absorption.¹⁹ However, this geometry was found to be problematic for planar on-chip waveguides owing to the submerged 2DES constituting a lossy ground plane which disrupts the guided modes. Furthermore, the layer arrangement makes it impossible to isolate specific areas of 2DES from the PC switches and the rest of the waveguide. We therefore designed a structure (Figure 3) in which the 2DES is grown after (above) the LT-GaAs layer, separated by a 500-nm-thick undoped GaAs buffer. The 2DES growth temperature ($575\ \text{°C}$) was carefully chosen to serve as a post-growth anneal of the LT-GaAs (grown at $180\ \text{°C}$), and to prevent the formation of long-lifetime carriers in the PC material. Further layers, introduced to aid fabrication and device

performance, included: a 500 nm GaAs buffer layer to prevent crystal imperfections from the LT-GaAs propagating through the heterostructure and affecting the overlaid 2DES heterostructure layer quality; a 100 nm AlAs layer between the GaAs buffer and LT-GaAs to form an etch stop for device processing; and a second, 400 nm AlAs layer beneath the LT-GaAs to prevent long-lifetime carrier excitation / recombination in the GaAs substrate. The presence of PC material across the entire substrate removes the need for epitaxial transfer of LT-GaAs onto a host substrate,¹⁹ significantly decreasing fabrication time and complexity, whilst maintaining an epitaxially perfect PC layer for improved THz generation.

III. RESULTS

A. Characterisation

To characterise the integrated layer structure, independent measurements of both the LT-GaAs and the 2DES quality were performed. First, a 100-nm-deep Hall bar mesa was etched into the surface of the 2DES-containing layers using a non-selective $\text{H}_2\text{SO}_4 : \text{H}_2\text{O}_2 : \text{H}_2\text{O}$ etch, with AuGeNi used to form ohmic contacts to the buried 2DES. Magnetotransport measurements were performed in a 1.2 K helium cooled bath cryostat with magnetic fields up to 6 T, and a sheet electron density of $3.4 \times 10^{11} \text{ cm}^{-2}$ and corresponding mobility of $0.5 \times 10^6 \text{ cm}^2\text{V}^{-1}\text{s}^{-1}$ were extracted. Second, a CPW device (Figure 2) was fabricated by removing the 2DES heterostructure in a selective citric acid : $\text{H}_2\text{O}_2 : \text{H}_2\text{O}$ etch which terminated at the 100 nm AlAs etch stop above the LT-GaAs layer. This was subsequently removed in dilute HF to reveal a perfect LT-GaAs layer beneath, on which the CPW was formed without further etching.

The CPW device was mounted in and thermally heat sunk to the holder shown in Figure 1, and electrical connections were made using phosphor-bronze wires arranged into twisted pairs. Measurements of the output pulse taken at room temperature demonstrated a transmitted pulsewidth of 3.8 ps, corresponding to a bandwidth of ~ 600 GHz. The lower than expected (1 THz)

bandwidth is likely to be a result of several factors, including the non-zero conductivity of the LT-GaAs substrate, as well as both radiative and resistive losses. Nevertheless, the individual characteristics of the 2DES and LT-GaAs in the monolithically-grown wafer are comparable to those of separately grown 2DES heterojunctions and LT-GaAs wafers.

This CPW (with the 2DES heterostructure removed) was next used to characterise the dilution refrigerator assembly. Upon cooling, misalignment arising from relative movement between the sample and fibres was corrected using the piezoelectric stages to maximise the PC switch photocurrent. Figure 4a shows input (between switches 1 and 2; Figure 2) and output (switches 1 and 3) pulse measurements performed at 200 mK (measured using a RuO₂ thermometer located at the sample plate), with the latter achieved by translating the probe beam to the required PC switch using the piezoelectric stages. No changes to the generated or transmitted THz pulse shapes were observed upon application of a transverse magnetic field, though a small (< 5%) decrease in THz pulse amplitude was observed at high (> 5 T) fields. This field dependence is attributed to competition between the Lorentz and electric forces exerted on the carriers in the biased PC switches under magnetic field, which therefore reduces the number of carriers available to contribute to the generated signal.³ To demonstrate further the versatility of the system, the probe beam was returned to the output pulse measurement configuration, and the excitation photocurrent was recorded as a function of pump beam position on the excitation switch (Figure 4b), whilst simultaneously mapping the transmitted THz amplitude at a fixed position on the probe switch (Figure 4c). These measurements were taken at a refrigerator temperature of 400 mK, limited predominantly by thermal loading from the stages during the stepped-raster scan, and at 12 T applied magnetic field. When the piezoelectric stages are not being stepped, the fridge temperature was ~200 mK, limited now by thermal loading from the NIR incident laser beams (a base temperature of < 27 mK was recorded in the absence of laser excitation).

B. Pulse injection

To investigate THz pulse injection into the 2DES layer, a new device was fabricated from the monolithically grown wafer. A 100-nm-deep etch was used to define a $120\ \mu\text{m} \times 30\ \mu\text{m}$ mesa. AuGeNi ohmic contacts measuring $10\ \mu\text{m} \times 10\ \mu\text{m}$ were deposited at each end of the mesa and annealed to provide ohmic contacts to the 2DES. The 2DES mesa was then protected using photoresist to prevent over-etching, allowing a surrounding larger mesa ($800\ \mu\text{m} \times 1000\ \mu\text{m}$) to be etched to expose the underlying LT-GaAs for THz generation and detection. A CPW structure containing a $100\ \mu\text{m}$ gap in the center conductor was then fabricated on the device, with each side of the gap connected to the ohmic contacts (Figure 5). Discontinuous ground planes were also introduced to suppress direct coupling of both the slotline and coplanar modes across the center-conductor gap, without interaction with the mesa. Initial measurements were performed by free-space optical excitation of the PC switches through the windows of a continuous flow helium cryostat, which allowed the device temperature to be swept controllably from room temperature down to $\approx 4\ \text{K}$. Pump and probe beam powers of 10 mW were used in this system to improve the signal-to-noise ratio (SNR) of THz pulses propagating through the 2DES mesa. The input and output pulses at room temperature and at 4K are given in Figures 6a and 6b, respectively.

It can be seen that the transmitted pulse amplitude increases significantly upon cooling. Further measurements demonstrated that, whilst the slotline component of the transmitted pulse (as a percentage of the measured input pulse) remains constant (and negligible) with temperature, the coplanar mode increased in amplitude as the sample is cooled (Figure 6b, inset). As the DC resistance of the 2DES reduces from $\approx 4\ \text{k}\Omega$ at room temperature (measured across the CPW center conductor gap) to $\approx 200\ \Omega$ at 4 K, the now highly conducting 2DES constitutes a continuation of the CPW center conductor and therefore supports coplanar mode propagation across the gap. The gap itself then acts as a low-pass filter, preventing short-wavelength, high-frequency

components from propagating, and therefore significantly reduces the transmitted pulse bandwidth (to ~ 250 GHz) and amplitude (to 8 nA, $\sim 30\%$ of the input pulse amplitude).

Subsequent measurements were taken in the dilution refrigerator at a fridge temperature of 200 mK, using 1 mW NIR excitation and detection powers. The PC photocurrent was optimised as previously using the piezoelectric stages to maximise THz generation and detection efficiency. No further increase in the transmitted THz pulse amplitude at 200 mK was observed, from the previous 4 K measurements, although a reduction in the absolute transmitted THz pulse amplitude from ~ 8 nA to < 400 pA (owing to the reduced laser power), and correspondingly reduced signal-to-noise ratio, may have masked further changes. The magnetic field was then swept from 0 – 1 T in 0.01 T steps, and the corresponding transmitted THz amplitude recorded. The results show a decreasing amplitude with increasing magnetic field, corresponding to the increasing DC resistance of the 2DES (Figure 6c). The expected low-field oscillations in the two-terminal DC resistance as the system approaches the quantum Hall regime can be seen above 0.5 T (solid line, Figure 6c). However, the low transmitted THz power and correspondingly poor signal-to-noise ratio, screen any observable oscillations in the transmitted THz pulse amplitude in this measurement.

IV. CONCLUSIONS

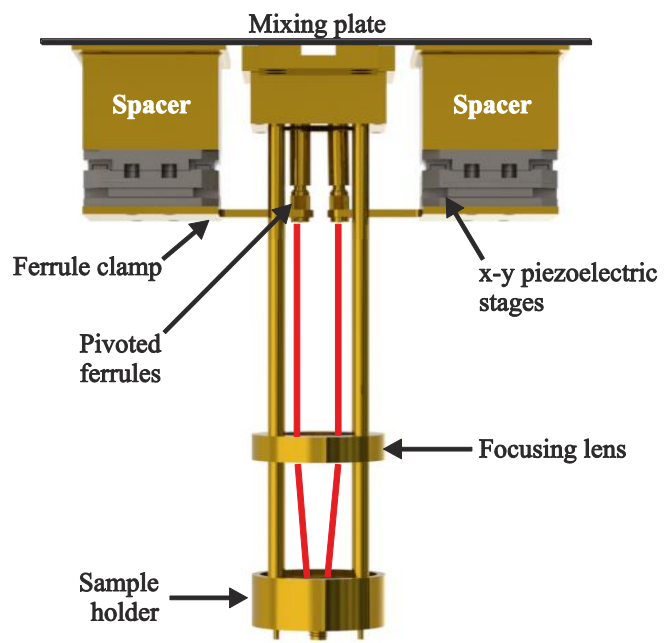
In this paper, we have presented a new experimental apparatus, which offers unprecedented control of the excitation and detection of on-chip guided wave THz signals within a dilution refrigerator at temperatures below 400 mK. The non-contact excitation allows for compensation of thermal drift during cooling, enabling repeatable and reproducible measurements to be taken from a single device. Furthermore, it is possible to measure both input and output THz transients in a single thermal cycle using precision, piezoelectric-controlled translation of the NIR excitation and detection pulses across the sample. This dynamic scanning capability, which also allows

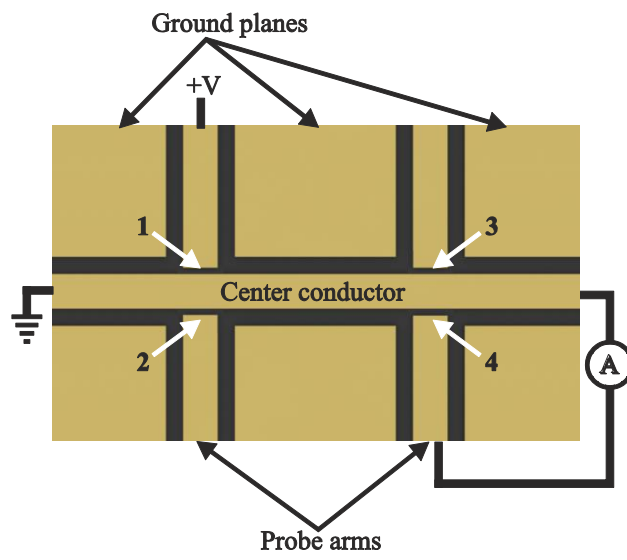
spatially-dependent THz transients to be excited and mapped on a device, is not limited to two-port device measurements such as those presented here, but has the potential to be used in more complex, multi-port devices, such as on-chip THz multiplexers, de-multiplexers and interferometers.

We have also developed a new monolithically integrated layer structure, grown by molecular beam epitaxy, which allows the direct integration of an on-chip waveguiding device with a single low-dimensional system for the measurement of ultra-fast carrier dynamics in mesoscopic environments. This will allow the study THz-frequency magnetoplasmon oscillations, and other dynamic carrier properties of 2DES structures. Furthermore, the subsequent ability to pattern the 2DES with, for example, surface Schottky gates opens up the possibility of measuring the THz conductivity of a wide range of nanoscale and mesoscopic systems.

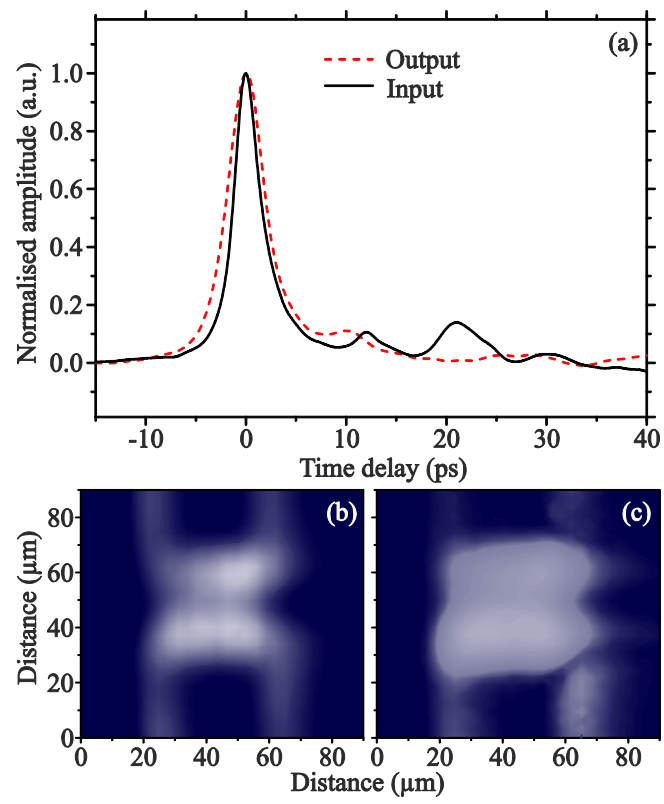
ACKNOWLEDGMENTS

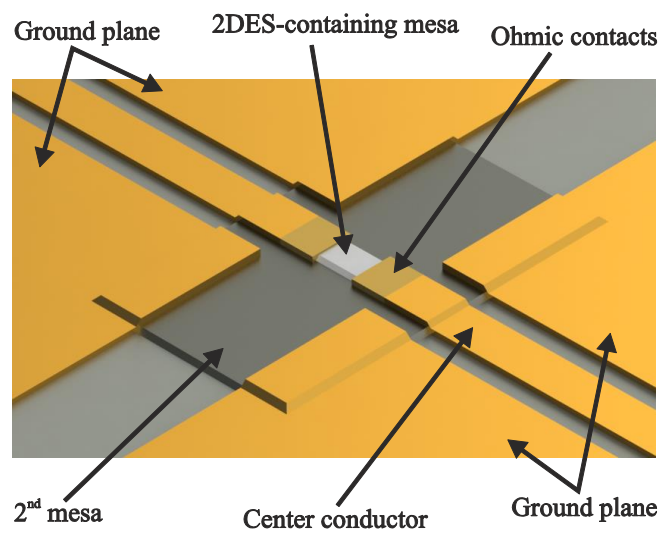
This work was funded by the Engineering and Sciences Physical Research Council, UK (EP/F029543/1). We also acknowledge support from the European Research Council programmes *NOTES* and *TOSCA*, the Royal Society and the Wolfson Foundation.





GaAs (10 nm)	} 2DES heterostructure
n-doped AlGaAs (40 nm)	
AlGaAs (20 nm)	
GaAs buffer (500 nm)	} On-chip Thz waveguide structure
AlAs etch stop (100 nm)	
LT-GaAs (2000 nm)	
AlAs optical barrier (400 nm)	
SI GaAs substrate	





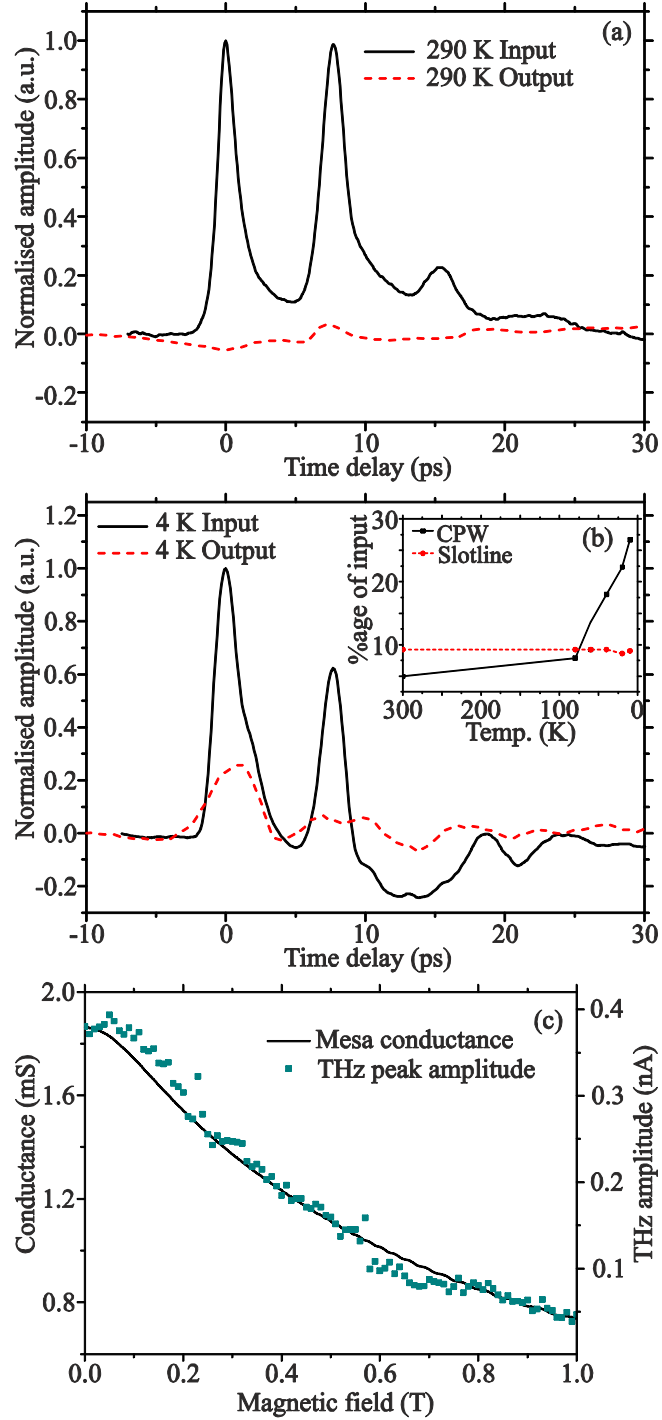


Figure captions:

FIG 1: THz excitation and detection apparatus located inside the dilution refrigerator.

FIG 2: Schematic diagram of a THz CPW formed on a continuous LT-GaAs surface (dark regions) comprising a gap – center conductor – gap of dimensions $20\ \mu\text{m} - 30\ \mu\text{m} - 20\ \mu\text{m}$. PC switches 1 – 4 are defined by $30\text{-}\mu\text{m}$ -width probe arms, separated from the ground planes by a $5\ \mu\text{m}$ gap. Switch pairs are separated by $1.2\ \text{mm}$.

FIG 3: The layer structure of a 2DES heterostructure monolithically integrated with a photoconductive LT-GaAs layer, grown by MBE.

FIG 4: a) Input (solid) and output (dashed) THz pulses measured in the dilution refrigerator at $200\ \text{mK}$ (pulse delay artificially removed for comparison); b) and c) spatial maps recorded at $400\ \text{mK}$ and $12\ \text{T}$ magnetic field, of the pump switch photocurrent and the corresponding peak-to-peak transmitted THz signal amplitude, respectively.

FIG 5: A THz CPW with a 2DES mesa integrated into the center conductor. The second mesa is present to prevent over-etching of the 2DES region when etching down to the LT-GaAs surface.

FIG 6: Input (solid) and output (dashed) THz pulses measured at: a) room temperature and b) $4\ \text{K}$, respectively; Inset b): area under the output pulse as a percentage of the input pulse for the slotline (circles) and coplanar (squares) guided modes, as a function of temperature; and c) transmitted THz signal amplitude as a function of magnetic field (symbols) compared with the 2-terminal mesa resistance (line), measured at a dilution refrigerator temperature of $200\ \text{mK}$.

- ¹. X. Wang, D. J. Hilton, L. Ren, D. M. Mittleman, J. Kono and J. L. Reno, *Opt. Lett.* **32** (13), 1845 (2007).
- ². E. A. Shaner and S. A. Lyon, *Phys. Rev. B.* **66**, 041402 (2002).
- ³. G. Ernst, R. J. Haug, M. Klingenstein, J. Kuhl, K. von Klitzing and K. Eberl, *Appl. Phys. Lett.* **68**, 3752 (1996).
- ⁴. P. Orellana and F. Claro, *Appl. Phys. Lett.* **75**, 1643 (1999).
- ⁵. E. A. Shaner and S. A. Lyon, *Phys. Rev. Lett.* **93** (3), 037402 (2004).
- ⁶. P. G. Huggard, J. A. Cluff, C. J. Shaw, S. R. Andrews and E. H. Linfield, *Appl. Phys. Lett.* **71**, 2647 (1997).
- ⁷. J. Kröll, J. Darmo, S. S. Dhillon, X. Marcadet, M. Calligaro, C. Sirtori and K. Unterrainer, *Nature* **449**, 698 (2007).
- ⁸. D. G. Cooke, F. A. Hegmann, Y. I. Mazur, W. Q. Ma, X. Wang, Z. M. Wang, G. J. Salamo, M. Xiao, T. D. Mishima and M. B. Johnson, *Appl. Phys. Lett.* **85** (17), 3839 (2004).
- ⁹. T. Müller, W. Parz, K. Unterrainer, S. Sauvage, J. Houel, P. Boucaud, A. Miard and A. Lemaître, *Phys. Rev. B.* **77**, 035314 (2008).
- ¹⁰. M. C. Nuss, P. M. Mankiewich, R. E. Howard, B. L. Straughn, T. E. Harvey, C. D. Brandle, G. W. Berkstresser, K. W. Goossen and P. R. Smith, *Appl. Phys. Lett.* **54**, 2265 (1989).
- ¹¹. C. Wood, J. Cunningham, P. C. Upadhyya, E. H. Linfield, I. C. Hunter and A. G. Davies, *Appl. Phys. Lett.* **88**, 142103 (2006).
- ¹². D. R. Grischkowsky, *IEEE. J. Select. Top. Quantum Electron.* **6** (6), 1122 (2000).
- ¹³. J. C. Burton, E. van Cleve and P. Taborek, *Cryogenics* **51**, 209 (2011).
- ¹⁴. S. Verghese, N. Zamdmer, Q. Hu and A. Förster, *Appl. Phys. Lett.* **70**, 2644 (1997).
- ¹⁵. M. Griebel, J. H. Smet, J. Kuhl, K. von Klitzing, D. C. Driscoll, C. Kadow and A. C. Gossard, *Appl. Phys. Lett.* **82**, 2179 (2003).
- ¹⁶. Grischkowsky D., Keiding S., van Exeter M., Fattinger C., *J. Opt. Soc. Am. B* **7** (10), 2006 (1990).
- ¹⁷. N. Zamdmer, Q. Hu, K. A. McIntosh and S. Verghese, *Appl. Phys. Lett.* **75**, 2313 (1999).
- ¹⁸. N. Zamdmer, Q. Hu, S. Verghese and A. Förster, *Appl. Phys. Lett.* **74**, 1039 (1999).
- ¹⁹. J. Cunningham, P. C. Upadhyya, C. K. Tiang, M. Lachab, S. Khanna, E. H. Linfield and A. G. Davies, *Semicond. Sci. Technol.* **22**, 811 (2007).
- ²⁰. J. Cunningham, C. Wood, A. G. Davies, I. Hunter, E. H. Linfield and H. E. Beere, *Appl. Phys. Lett.* **86**, 213503 (2005).